Spectroscopic study of ^{50}V

Arkadip Bera,[1] Abhijit Bisoi,[1,*] Y. Sapkota,[2] Rozina Rahaman,[1] Anik Adhikari,[1] Arkabrata Gupta,[1] Ananya Das,[3] H. Ghosh,[1] S. Sarkar,[1] Dibyadyuti Pramanik,[4] Sangeeta Das,[1] Sathi Sharma,[5] S. Ray,[6] Shabir Dar,[7,8] S. Nandi,[7,8,†] S. Bhattacharya,[7,8] T. Bhattacharjee,[7,8] G. Mukherjee,[7,8] S. Bhattacharyya,[7,8] S. Samanta,[9,‡] S. Das,[9] S. Chatterjee,[9] R. Raut,[9] and S. S. Ghugre[9]

[1]*Indian Institute of Engineering Science and Technology, Shibpur, Howrah 711103, India*
[2]*Department of Physics, Dudhnoi College, Dudhnoi, Goalpara, Assam 783124, India*
[3]*Dream Institute of Technology, Samali, Kolkata 700104, India*
[4]*Haldia Institute of Technology, Haldia 721657, India*
[5]*Department of Physics, Manipal University Jaipur, Jaipur 303007, India*
[6]*Amity Institute of Nuclear Science and Technology, Amity University, Noida, Uttar Pradesh 201313, India*
[7]*Variable Energy Cyclotron Centre, 1/AF Bidhannagar, Kolkata 700064, India*
[8]*Homi Bhabha National Institute, Training School Complex, Anushaktinagar, Mumbai 400094, India*
[9]*UGC-DAE Consortium for Scientific Research, Kolkata Centre, Kolkata 700098, India*

High-spin positive parity states of ^{50}V, populated through the ^{48}Ti(^{4}He, np)^{50}V reaction with a 48 MeV α beam, have been studied using the Indian National Gamma Array (INGA) facility. A few new levels and γ-ray transitions have been added to the level scheme utilizing the results of intensity, directional correlation, and linear polarization measurements. Lifetimes of a few excited states have been measured for the first time using the Doppler shift attenuation method (DSAM). Large basis shell model calculations have been performed within the fp valence space to understand the microscopic origin of the excited states. Apart from the ground state yrast band [having a $\pi(1f_{7/2}^3) \otimes \nu(1f_{7/2}^7)$ particle configuration], a non-yrast band with a $\pi(1f_{7/2}^3) \otimes \nu(1f_{7/2}^6, 2p_{3/2}^1)$ particle configuration has also been identified. The interplay between single-particle and collective modes of excitation have been investigated in the observed bands by analyzing the particle partitions and spectroscopic quadrupole moments, both calculated using large basis shell model calculations.

I. INTRODUCTION

The field of γ-ray spectroscopy has witnessed unprecedented development over the last few decades. State-of-the-art experimental facilities, coupled with unparalleled advancements in computational power, have revolutionized the field in multiple ways. These have led to the realization of the most exotic nuclear shapes at the extremes of spins and isospins. Owing to the same advancements, a renewed interest in the low-mass region of the Segrè chart has also resurfaced simultaneously. Of particular interest in the low-mass region is the $1f_{7/2}$ subshell. The $1f_{7/2}$ subshell has properties unique to this mass region. It is bounded by two doubly-magic nuclei, ^{40}Ca and ^{56}Ni. Considering an inert ^{40}Ca core, the number of valence particles/holes in the middle of this subshell is eight, large enough to generate a collective behavior of the nucleons, giving the nucleus a deformed shape. Deformation near the ground state thus increases as one moves towards the middle of the subshell, which again decreases towards the end [1–5]. As a result, the $1f_{7/2}$ subshell is an ideal playground to look for the coexistence of and interplay between the two predominant modes of nuclear excitation: single particle and collective. In this regard, the self-conjugate nucleus, ^{48}Cr, lying in the middle of the $1f_{7/2}$ subshell, was one of the earliest nuclei to be investigated. ^{48}Cr shows a large deformation ($\beta = 0.28$) near the ground state [2,3]. Several nuclei around the ^{48}Cr nucleus also show collective excitation in the form of rotational-like band structures in their level schemes [6,7]. This interplay between single-particle and collective excitations in the $1f_{7/2}$ subshell nuclei has also been successfully explained by shell model calculations [8–10].

In a recent work, we reported on the structural evolution of the nucleus ^{49}V [11], which lies near the middle of the $1f_{7/2}$ subshell. In the same experiment, carried out using an alpha beam, the nucleus ^{50}V was also populated significantly. Within the framework of the zero-order shell model, ^{50}V has ten nucleons (three protons + seven neutrons) in the $1f_{7/2}$ subshell. The literature on ^{50}V contains studies conducted using light-ion beams such as proton [12], deuteron [13], triton [14], alpha [15,16], and ^{3}He [17,18]. Its highest energy level exists at an excitation energy of 12.57 MeV, found in a

^{51}V(p, d) ^{50}V reaction [12]. The data on heavy-ion induced reaction for ^{50}V are not available in the evaluated (ENSDF) as well as the unevaluated (XUNDL) datasets of NNDC [19]. The last reported study on this nucleus using an alpha beam was carried out by Giorni *et al.* [15] and Kennedy *et al.* [16] separately but concurrently. Giorni *et al.* extended the level scheme of ^{50}V up to the band-terminating state ($J^\pi = 11^+$) at 4.29 MeV and assigned the spins and parities of the levels. They measured the multipole mixing ratios (δ) of a few magnetic dipole transitions. Also, they reported the measured lifetimes of all the levels of the ground state dipole band in the same work. However, the uncertainties in these reported lifetimes are significant, more than 100% in most cases. In addition, the lifetimes of the 910.4 keV (7^+) and 1725.1 keV (8^+) levels differ significantly from the values reported by Kennedy *et al.* [16]. The report of Kennedy *et al.* comprises lifetime measurements of seventeen levels up to 1.88 MeV excitation energy with lesser uncertainties, including those due to stopping powers.

The primary motivation of this work is to expand the level scheme of ^{50}V, followed by lifetime measurements of newly observed and existing levels with better precision, and to carry out a detailed theoretical investigation through microscopic calculations. Thus, the present work investigates the different modes of excitation of the ^{50}V nucleus, populated through an α-beam induced reaction. The existing level scheme was modified up to the 6.10 MeV level by adding a few levels and transitions. Using the Doppler shift attenuation method (DSAM), the lifetimes of four levels were measured for the first time, and those of four other levels were remeasured to reduce the previously reported uncertainties. Relative intensity, directional correlation, and polarization measurements were carried out for the decay out transitions to assign the spins and parities of the new levels. Large basis shell model (LBSM) calculations were carried out to understand the microscopic origin of the levels of interest and to interpret the observed results.

The paper is organized as follows. The experiment and the data analysis techniques employed are outlined, followed by the experimental results and their interpretation, and finally the theoretical investigations are discussed.

II. EXPERIMENTAL DETAILS AND DATA ANALYSIS

The ^{48}Ti(^{4}He, np) ^{50}V fusion evaporation reaction was used to populate high-spin states of ^{50}V. The experiment was carried out during the second phase of the Indian National Gamma Array (INGA) campaign at the Variable Energy Cyclotron Centre (VECC), Kolkata. A 48 MeV ^{4}He beam was supplied by the K-130 Cyclotron stationed at VECC. A self-supported 12.4 mg/cm^2 thick natural Ti target was used, within which $\approx$95% of the recoils stopped. The multidetector array, INGA, was used to detect the deexciting γ rays following the reaction. The INGA setup, during the present experiment, comprised six Compton-suppressed clovers and two low-energy photon spectrometers (LEPS). Out of the six clovers, two were mounted at 125°, three at 90°, and one at 40° with respect to the beam axis. The two LEPS were mounted at 90° and 40° with respect to the beam axis. Singles and two-

fold γ-γ coincidence events were recorded in list mode using a digital data acquisition system. The pulse processing and data acquisition system was that of UGC-DAE CSR, Kolkata Centre, and was based on the 250 MHz 12-bit PIXIE 16 digitizers (XIA LLC) [20]. The coincidence data were sorted using the sorting program IUCPIX [20] to generate symmetric and asymmetric matrices, which were then analyzed using the program INGASORT [21].

As the transition energies relevant to the current work are more than 1500 keV, the energy calibrations of the clovers were performed with a few online γ rays, in addition to the standard ^{152}Eu and ^{133}Ba radioactive sources which emit γ rays up to a maximum of 1408 keV. The online γ rays chosen for the energy calibration comprised a few well-separated, stopped (with no Doppler-broadening or shift) peaks having energies ranging from 400 through 2100 keV, corresponding to known γ-ray transitions populated via other reaction channels. The high-energy room background γ rays (like 2614 keV) could not be considered due to their low statistics. The relative efficiency calibrations of the clovers were performed up to 4.8 MeV with ^{152}Eu and ^{66}Ga radioactive sources. The ^{66}Ga source was prepared through the ^{56}Fe(^{13}C, $p2n$) ^{66}Ga reaction at 50 MeV [22]. The efficiency uncertainty was estimated by fitting the efficiency curve in INGASORT [21].

In order to build up the level scheme, the raw data were sorted into angle-independent and angle-dependent (90° vs 90°) symmetric, and asymmetric γ-γ coincidence matrices. The angle-dependent symmetric matrix was used to measure the relative intensities of the γ-ray transitions. An asymmetric matrix was used to assign the spins of excited levels from the results of DCO measurements. DCO stands for directional correlation of γ rays deexciting oriented states, and is represented as a ratio, R_{DCO}. The R_{DCO} of a γ-ray transition is defined as the ratio of its intensity measured at two different angles in coincidence with another γ-ray transition of known multipolarity [23],

$$R_{\text{DCO}} = \frac{I^{\gamma_1} \text{ observed at } \theta_1, \text{ gated by } \gamma_2 \text{ at } \theta_2}{I^{\gamma_1} \text{ observed at } \theta_2, \text{ gated by } \gamma_2 \text{ at } \theta_1}.$$

For the present setup, DCO ratios were determined for $\theta_1 = 125°$ and $\theta_2 = 90°$ (Table I). For a pure dipole (quadrupole) transition gated by a pure quadrupole (dipole) transition, R_{DCO} is close to 0.7 (1.41). For a transition gated by another transition of the same multipolarity, R_{DCO} is close to unity. R_{DCO} values may deviate from the above values depending on the amount of mixing present in the transitions. In the present work, R_{DCO}'s were measured mostly from 754 and 910.4 keV gated spectra. Both 754 and 910.4 keV transitions are magnetic dipole in nature with mixing ratios, $\delta = -0.13^{+0.09}_{-0.05}$ and $-0.21^{+0.10}_{-0.16}$, respectively [15]. As a result, the calculated R_{DCO} of a pure dipole (quadrupole or $\Delta J = 0$) transition gated by the 754 keV transition as obtained from the computer code ANGCOR [23] is $1.08^{+0.03}_{-0.05}$ ($1.59^{+0.06}_{-0.13}$). On the other hand, the calculated R_{DCO} of a pure dipole (quadrupole or $\Delta J = 0$) transition gated by the 910.4 keV transition is $1.13^{+0.08}_{-0.06}$ ($1.72^{+0.20}_{-0.13}$) [23].

Integrated polarization directional correlation from oriented nuclei (IPDCO) [24] measurements were performed to

TABLE I. Relative intensity (I_{rel}), R_{DCO}, and Δ_{IPDCO} of γ-ray transitions in ^{50}V. Note that 7_3^+ and 7_4^+ levels could not be identified in the present experiment. Identification of the positions of different 7^+ levels are discussed in the text.

E_X (keV)	E_γ (keV)	I_{rel}	J_i	J_f	Gating γ[a] (keV)	R_{DCO}	Δ_{IPDCO} Expt.	Δ_{IPDCO} Theor.	Multipolarity
910.4(4)	910.4(4)	100(6)	7_1^+	6_1^+	754	0.93(7)	−0.03(1)	−0.02	$M1 + E2$
1725.1(7)	814.7(4)	72(5)	8_1^+	7_1^+	910.4	1.09(8)	−0.03(1)	−0.02	$M1 + E2$
	1725.1(7)	39(5)	8_1^+	6_1^+	754	1.5(2)	0.08(2)		$E2$
1761.5(6)	851.1(6)	1.0(3)	$(6)_2^+$	7_1^+					$(M1 + E2)$[b]
2313.2(6)	588.1(6)	2.5(3)	$(7)_2^+$	8_1^+	910.4	1.3(2)	−0.13(4)		$M1 + E2$
2479.1(4)	754.0(4)	44(4)	9_1^+	8_1^+	910.4	1.08(9)	−0.04(1)	−0.03	$M1 + E2$
2841.2(11)	1930.8(11)	9.9(9)	8_2^+	7_1^+	910.4	1.2(2)	−0.05(3)		$M1 + E2$
3475.4(20)	2565(2)	5.7(7)	7_5^+	7_1^+	910.4	2.0(5)	0.09(6)		$M1 + E2$
	3475(2)	10.4(14)	7_5^+	6_1^+	613.2	0.9(3)	−0.10(9)		$M1 + E2$
3730.5(4)	1251.4(4)	24(2)	10_1^+	9_1^+	910.4	0.95(9)	−0.03(1)	−0.03	$M1 + E2$
3747.2(8)	1268.1(8)	3.0(4)	$(9^+)_2$	9_1^+					$(M1 + E2)$[b]
4088.3(13)	1609.2(13)	6.3(6)	$(9)_3^+$	9_1^+	754	1.5(2)	0.10(4)		$(M1 + E2)$
4088.6(5)	613.2(5)	3.7(4)	8_3^+	7_5^+	910.4	1.2(2)	−0.14(4)		$M1 + E2$
4293.4(4)	562.9(4)	11.1(9)	11^+	10_1^+	910.4	1.1(2)	−0.07(2)	−0.05	$M1 + E2$
4420.4(20)	331.8(6)	1.8(2)	9_4^+	8_3^+	910.4	1.2(3)	−0.11(8)		$M1 + E2$
	673.2(7)	1.0(2)	9_4^+	$(9^+)_2$					$(M1 + E2)$[b]
	1579.2(9)	2.0(3)	9_4^+	8_2^+					$M1 + E2$[c]
	2695(2)	1.8(2)	9_4^+	8_1^+					$M1 + E2$[c]
5410.8(5)	990.4(5)	6.4(6)	10_2^+	9_4^+	910.4	1.1(2)	−0.08(3)		$M1 + E2$
5768.3(20)	1680(2)	3.7(4)	$(11)_2^+$	$(9)_3^+$	754	1.5(3)	0.11(4)		$(E2)$
	2038(2)	1.0(3)	$(11)_2^+$	10_1^+					$(M1 + E2)$[c]
6104.6(6)	693.8(6)	4.5(5)	11_3^+	10_2^+	910.4	1.2(3)	−0.14(5)		$M1 + E2$

[a] $\Delta J = 1$ transitions.
[b] Tentatively assigned based on theoretical results.
[c] Based on J_i^π and J_f^π.

assign the electric or magnetic nature of the transitions. Two asymmetric IPDCO matrices were constructed from the data for the purpose. The first (second) matrix, named parallel (perpendicular), was constructed having on the first axis the simultaneous events recorded in the two crystals of the 90° clovers, which are parallel (perpendicular) to the emission plane, and on the second axis the coincident γ ray registered in any other clover. The polarization asymmetry is defined as

$$\Delta_{IPDCO} = \frac{a(E_\gamma)N_\perp - N_\parallel}{a(E_\gamma)N_\perp + N_\parallel} \tag{1}$$

where $N_\perp$ and $N_\parallel$ are the intensities of the full energy peaks observed in the perpendicular and parallel matrices, respectively. A positive (negative) value of Δ_{IPDCO} indicates a pure electric (magnetic) transition. The Δ_{IPDCO} is close to zero for mixed transitions, and its sign may change depending on the amount of multipole mixing, δ. The correction term $a(E_\gamma)$ is introduced due to an asymmetry in the response of the different crystals of the clovers at 90°. It is defined as

$$a(E_\gamma) = \frac{N_\parallel(\text{unpolarized})}{N_\perp(\text{unpolarized})}. \tag{2}$$

In the present experiment, $a(E_\gamma)$ was measured as a function of the energies of unpolarized γ rays from a ^{152}Eu radioactive source. This correction term was close to unity (Fig. 1) in the entire energy range for the present INGA setup.

The theoretical Δ_{IPDCO} of a few dipole transitions with known multipole mixing ratios (δ) were calculated and compared with their experimental values (Table I). The formalism of Ref. [22] was used for the calculations. The polarization sensitivities, $Q(E_\gamma)$, of these transitions were estimated using
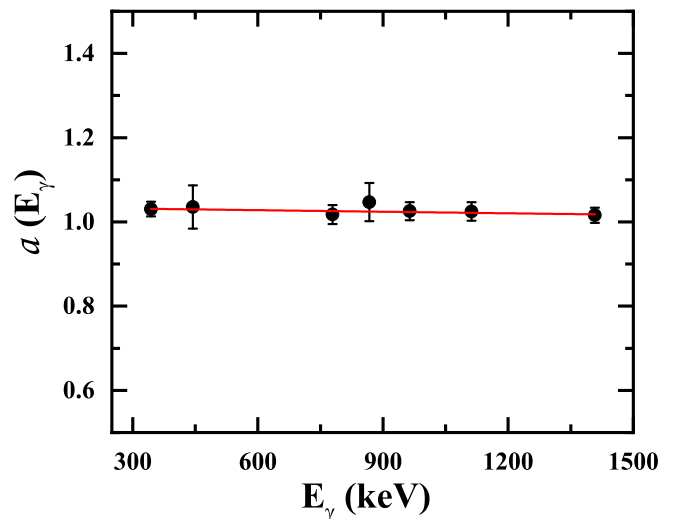

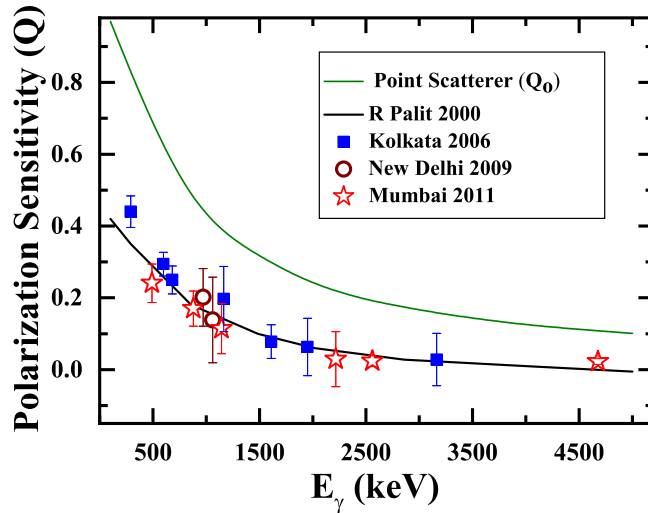FIG. 1. Asymmetry parameter $a(E_\gamma)$ plotted as a function of γ-ray energy for the present INGA setup.

FIG. 2. The polarization sensitivity (*Q*) of a clover detector measured as a function of γ-ray energy (i) in a measurement with single clover at similar distance [25] and at different implementations of INGA at (ii) Kolkata (2006) [26], (iii) New Delhi (2009) [27], and (iv) Mumbai (2011) [22].
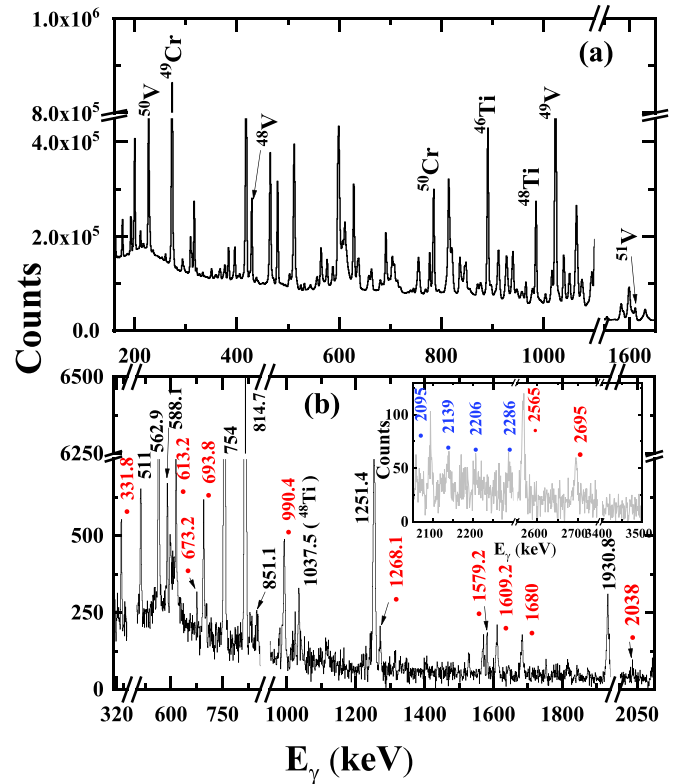

FIG. 3. (a) A background subtracted total projection spectrum of γ rays emitted by different nuclei formed in the present experiment. Only the strongest ground state transitions of the populated nuclei are marked. (b) Background subtracted coincidence spectrum obtained by putting a gate on the 910.4 keV transition. New transitions are marked by red asterisks. γ-ray energies from 2050 to 3500 keV are shown in the inset. Transitions that may likely belong to ^{50}V (not placed in the level scheme) are marked with blue diamonds. Spectra were generated from a 90° vs 90° symmetric matrix.

the relation previously obtained for similar clovers used in the INGA setup of Tata Institute of Fundamental Research (TIFR), Mumbai in 2011 (Fig. 2). The attenuated angular distribution coefficients were theoretically estimated from Ref. [28].

To carry out lifetime measurements using DSAM, two asymmetric matrices were constructed with events recorded by the clovers at a particular angle (125°, or 40°) on one axis, and the corresponding coincidence events recorded by the 90° clovers on the other to generate line-shape spectra. A modified version of the computer code LINESHAPE [29] was used to extract level lifetimes from the Doppler-shifted spectra. The initial recoil momenta distributions of ^{50}V were obtained from PACE4 [30] calculation. In the first step of the LINESHAPE program, the slowing-down histories of 50 000 ^{50}V recoiling nuclei in the natural Ti target were simulated using the Monte Carlo technique. The velocity profiles of the recoils were generated with a time step of 0.0007 ps. The geometry of the clovers were also taken into account. In the second step, using the stopping powers and the velocity distributions calculated in the first step, a line shape for each decay time was obtained. In the final step, utilizing a χ^2-minimization technique, the theoretically generated line shapes best fitted to the experimental ones were obtained. The γ-ray transition energies and the side-feeding intensities obtained from the measured relative intensities were used as the input parameters. In this measurement, shell-corrected Northcliffe and Schilling stopping powers [31] were used for calculating the energy loss of ions in matter.

III. RESULT AND DISCUSSION

A. Level Scheme

The present work is primarily concerned with the investigation of positive parity states of ^{50}V. As a natural Ti target was

used in the experiment, the cross section of ^{50}V as predicted by PACE4 [30] is only 4.6% of the total cross section. A background subtracted total-projection spectrum is shown in Fig. 3(a), where nuclei populated via different reaction channels are mentioned.

During the analysis, all existing transitions of ^{50}V [15] up to the $J^\pi = 11^+$ level were observed. In addition, thirteen new transitions were identified (indicated by asterisks and coloured red in the level scheme of Fig. 5). A 1932 keV transition was assigned tentatively in the level scheme of Ref. [15] using a dotted line. Its position in the level scheme was confirmed in the present work as a 1930.8 keV transition. All newly identified transitions were placed in the level scheme by testing different coincidence relationships using symmetric γ-γ coincidence matrices. Some relevant coincidence relationships are discussed below by making references to a few coincidence spectra [Figs. 3(b) and 4], where the newly observed transitions are indicated by asterisks and coloured red.

(i) Barring the 3475 keV transition, the remaining twelve transitions were observed in the 910.4 keV gated spectrum [Fig. 3(b)].
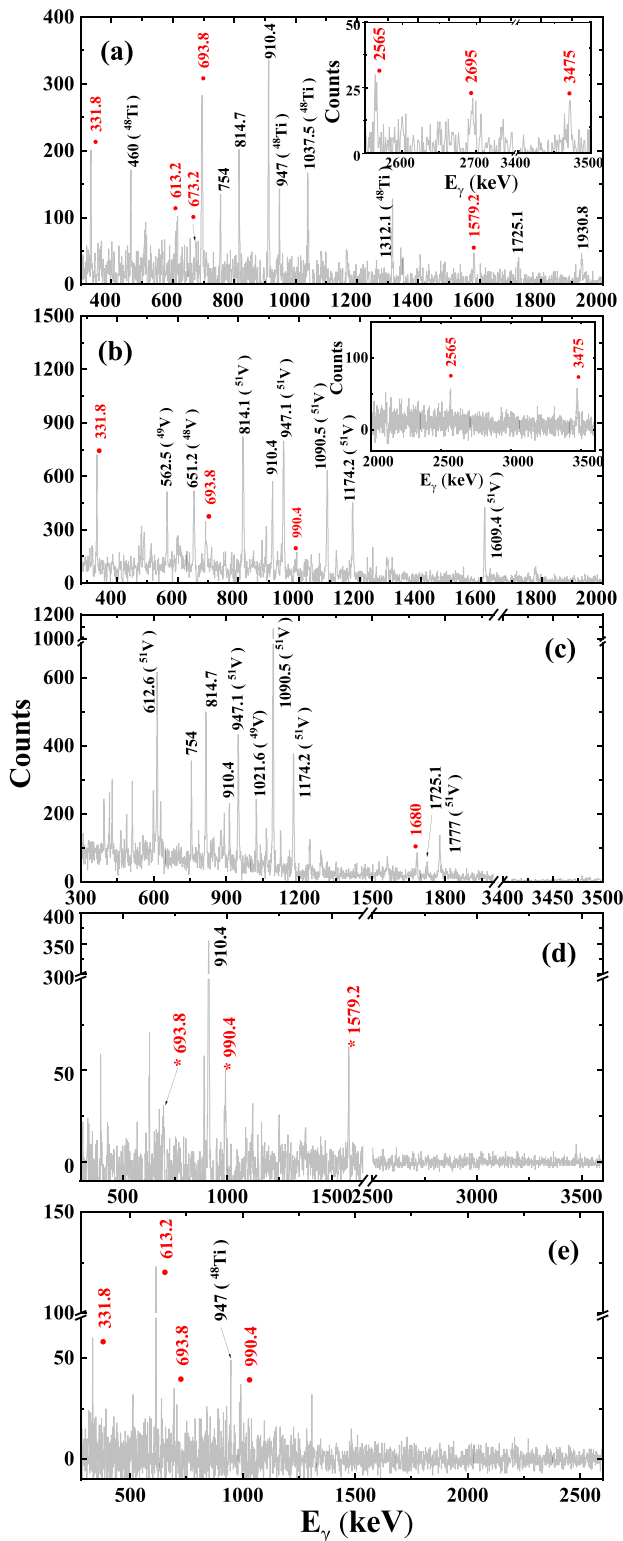
FIG. 4. Background subtracted coincidence spectrum obtained by putting a gate on (a) 990.4, (b) 613.2, (c) 1609.2, (d) 1930.8, and (e) 3475 keV transitions. New transitions are marked by red asterisks.

(ii) The newly observed 331.8, 613.2, 693.8, 990.4, and 2565 keV transitions were in coincidence with each other [Figs. 4(a) and 4(b)]. Among these, the 331.8, 613.2 [Fig. 4(b)], and 2565 keV transitions were

in coincidence neither with the 1579.2 or 1930.8 [Fig. 4(d)] keV transitions, nor with the 673.2 or 1268.1 keV transitions. These three transitions were not in coincidence with the 2695 keV transition also [Fig. 4(b)].

(iii) The 693.8 and 990.4 keV [Fig. 4(a)] transitions were in coincidence with the 673.2, 1268.1, 1579.2, and 1930.8 keV [Fig. 4(d)] transitions.

(iv) The 1579.2 and 1930.8 keV transitions were in coincidence with each other, but not in coincidence with the 673.2 and 1268.1 keV transitions [Fig. 4(d)].

(v) The 673.2 and 1268.1 keV transitions were in coincidence with each other and also observed in the 754, 814.7, and 910.4 keV [Fig. 3(b)] gated spectra.

(vi) The 1609.2 and 1680 keV transitions were in coincidence with each other [Fig. 4(c)] and were also observed in the 754, 814.7, and 910.4 keV [Fig. 3(b)] gated spectra. But they were not observed in the 331.8, 613.2 [Fig. 4(b)], 693.8, 990.4 [Fig. 4(a)], or 2565 keV gated spectra.

(vii) The 3475 keV transition was observed in the 990.4, and 613.2 keV gated spectra [Figs. 4(a) and 4(b)] but not observed in the 910.4 keV gated spectrum [Fig. 3(b)]. Transitions in coincidence with the 3475 keV transition are shown in Fig. 4(e).

Due to the presence of Doppler-broadening in a few transitions, the relative intensities of the γ-ray transitions were measured from a 90° vs 90° symmetric matrix (Table I). The relative intensities of most of the transitions were measured from a 910.4 keV gated spectrum. The relative intensity of the 910.4 keV transition was measured from the total projection
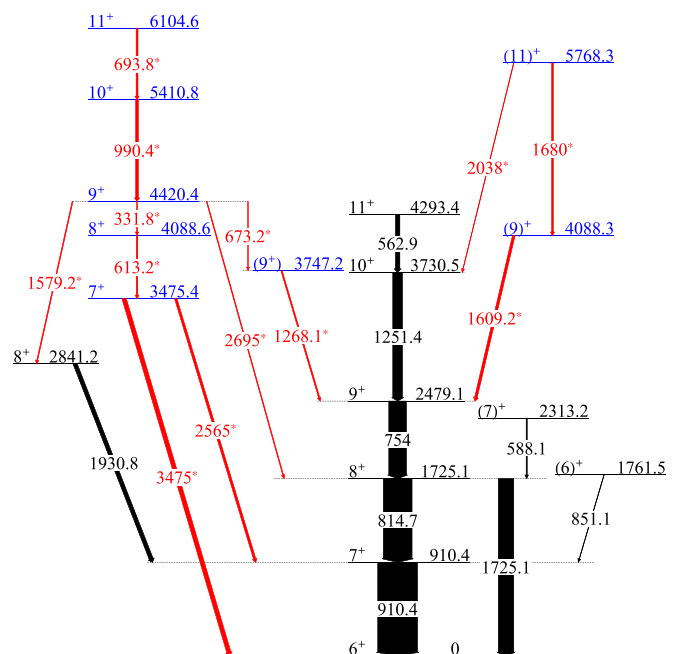

FIG. 5. Partial level scheme of ^{50}V. Only the levels of interest are shown in this figure. The newly observed transitions (red) are marked by red asterisks. New levels are marked in blue.

TABLE II. Experimental level lifetimes, experimental branchings, experimental and theoretical reduced transition probabilities ($B(EL)/B(ML)$) for different transitions are tabulated. The units of $B(M1)$, and $B(E2)$ are μ_N^2, and $e^2\mathrm{fm}^4$, respectively. Multipole mixing ratios (δ) obtained from shell model calculations are also tabulated.

E_X (keV)	τ_{mean} (fs) Present	Prev. [15]	Prev. [16]	J_i^π	J_f^π	E_γ (keV)	Branching (%)	Mixing ($|\delta|$) Prev. [15]	Theor.	$B(M1)$ Present	Theor.	$B(E2)$ Present	Theor.
910.4		120^{+120}_{-60}	62(11)	7_1^+	6_1^+	910.4	100	$0.21^{+0.16}_{-0.10}$	0.08	$1.15^{+0.29}_{-0.25}$ c	1.04	869^{+2142}_{-660} c	122
1725.1	626(192)	530^{+600}_{-200}	200(90)	8_1^+	7_1^+	814.7	65(5)	$0.17^{+0.15}_{-0.14}$	0.05	$0.11^{+0.06}_{-0.04}$	0.19	65^{+266}_{-63}	12
				8_1^+	6_1^+	1725.1	35(5)	$E2$	$E2$			30(13)	84
2313.2	<286			$(7)_2^+$	8_1^+	588.1	100		0.02	>0.96	0.77		14
2479.1	148(46)	350^{+400}_{-200}		9_1^+	8_1^+	754	100	$0.13^{+0.05}_{-0.09}$	0.05	$0.87^{+0.41}_{-0.22}$	1.35	367^{+637}_{-340}	79
2841.2	366(146)			8_2^+	7_1^+	1930.8	100		0.33	0.02(1)	0.17		69
3730.5	52(16)	40^{+80}_{-35}		10_1^+	9_1^+	1251.4	100	$0^{+0.07}_{-0.04}$	0.07	$0.55^{+0.24}_{-0.13}$	1.22		50
4088.3	79(30)			$(9)_3^+$	9_1^+	1609.2	100		0.13	0.16(7)	0.10		9
4293.4	<300	350(100)		11_1^+	10_1^+	562.9	100	$0.06^{+0.01}_{-0.06}$	0.03	>1.04	1.07	>168	33
5768.3	<223			$(11)_2^+$	$(9)_3^+$	1680	79(9) b		$E2$			>211	50
3475.4	63 a			7_5^+	6_1^+	3475	65(6)		0.51		0.01		3.4
4088.6	1517 a			8_3^+	7_5^+	613.2	100		0.04		0.16		12
4420.4	576 a			9_4^+	8_3^+	331.8	29(3)		0.03		0.77		127
5410.8	67 a			10_2^+	9_4^+	990.4	100		0.11		0.85		156
6104.6	274 a			11_3^+	10_2^+	693.8	100		0.08		0.61		111

[a] Calculated lifetime.

[b] Estimated from the relative intensities.

[c] From Ref. [16].

spectrum with proper normalization. Relative intensities for the transitions parallel to the 910.4 keV transition (viz., 1725.1 and 3475 keV) were measured from the branching ratios of the respective levels. The relative intensities of these transitions were not measured from the total projection spectrum due to their low statistics. Necessary correction due to the angular distributions of dipole and quadrupole transitions at 90° was taken care of in the present measurement. All new transitions were placed in the level scheme (Fig. 5) based on their coincidence relationships and relative intensities. As a result, eight new levels, viz., 3475.4, 3747.2, 4088.3, 4088.6, 4420.4, 5410.8, 5768.3, and 6104.6 keV, were added to the existing level scheme (Fig. 5).

The spin and parity of the levels in ^{50}V were assigned/confirmed based on the results obtained from DCO and linear polarization measurements. The R_{DCO} and Δ_{IPDCO} values of 910.4, 814.7, 754, 1251.4, and 562.9 keV transitions confirmed the J^π assignment of the existing levels. A 2313.2 keV level was reported previously, but its spin and parity was not assigned. This 2313.2 keV level decays to the 1725.1 keV level via a 588.1 keV transition. In the present work, the R_{DCO} and Δ_{IPDCO} of the 588.1 keV transition were extracted, which confirmed the magnetic dipole nature of the 588.1 keV transition. Thus, the 2313.2 keV level could either be a 7^+ or a 9^+ level. In alpha induced reactions, non-yrast levels are populated heavily, and the associated level schemes get extended horizontally [32]. It was observed from shell model results (discussed later in Sec. IV A) that a 7^+ assignment was more appropriate than a 9^+ assignment for the 2313.2 keV level. Therefore, the spin and parity of the 2313.2 keV level were assigned a tentative $(7)^+$.

The R_{DCO} of the 1930.8 keV transition measured from the 910.4 gated spectrum was 1.2(2) and its Δ_{IPDCO} was negative,

indicating a magnetic dipole nature. So, the spin and parity of the 2841.2 keV level were assigned 8^+.

The spin and parity of 3475.4 keV level were assigned based on the R_{DCO} and Δ_{IPDCO} values of 613.2, and 3475 keV transitions. The R_{DCO} of 613.2, 331.8, 693.8, and 990.4 keV transitions are 1.2 (2), 1.2(3), 1.1(2), and 1.2(3), respectively (Table I) and all of them have negative Δ_{IPDCO} values. We used the 910.4 keV gated spectrum for the R_{DCO} measurement. 910.4 keV is a magnetic dipole transition with mixing (δ) $-0.21^{+0.10}_{-0.16}$ [15], and the R_{DCO} of a pure dipole (quadrupole) transition gated by the 910.4 keV transition is $1.13^{+0.08}_{-0.06}$ ($1.72^{+0.20}_{-0.13}$) as obtained from ANGCOR [23]. So, the above transitions are dipole transitions and may have very small mixing. The calculated mixings of these transitions (Table II) obtained from shell model calculations also support this observation. The R_{DCO} of the 3475 keV transition obtained from the 613.2 keV transition is close to unity and has negative Δ_{IPDCO} value, which therefore confirms its magnetic dipole nature. The 3475.4 keV level decays to the ground state ($J^\pi = 6^+$) through the 3475 keV transition. The spin and parity of the 3475.4 keV level is therefore assigned as 7^+. We have also calculated the R_{DCO} of 3475 keV gated by the 613.2 keV transition using the computer code ANGCOR [23]. In the calculation, we have considered both of them as $M1$ transitions, and the mixing values are taken from theoretical calculations (Table II). The calculated R_{DCO} value (0.83) also lies within the uncertainty of their measured value [0.9(3)] (Table I). The measured R_{DCO} and Δ_{IPDCO} of the 2565 keV ($\Delta J = 0$) transition decays from the 3475.4 keV level also support this assignment [33]. Based on the J^π of the 3475.4 keV level, the spins and parities of 4088.6, 4420.4, 5410.8, and 6104.6 keV levels were assigned as 8^+, 9^+, 10^+, and 11^+, respectively.

The R_{DCO} and Δ_{IPDCO} values of the 1609.2 keV transition (Table I) indicated that it was either a magnetic dipole ($\Delta J = 0$) or an electric quadrupole transition. So, the spin and parity of the 4088.3 keV level could be either 9^+ or 11^+. Similarly to the spin-parity assignment of the 2313.2 keV level based on shell model results, the 4088.3 keV level was assigned a tentative $(9)^+$. The spin and parity of the 5768.3 keV level were assigned based on the R_{DCO} and Δ_{IPDCO} values of the 1680 keV transition (Table I). As the J^π of the 4088.3 keV level was assigned a $(9)^+$, the spin and parity of the 5768.3 keV level were subsequently assigned $(11)^+$.

Kennedy *et al.* had assigned the spin and parity of the 1761.5 keV level as $(6, 7)^+$ [16]. It was mentioned in their work that the 1761.5 keV level could be a possible candidate for the second 6^+ level, as suggested by MBZ wave functions [34]. The 1761.5 keV level decays to the ground state, and to the 910.4 keV level through 1761.5 and 851.1 keV transitions, respectively [16]. In the present work, an 851.1 keV transition was seen in the 910.4 keV gated spectrum [Fig. 3(b)]. However, due to its low statistics and the presence of other contaminant transitions, the spin and parity of the 1761.5 keV level could not be confirmed. Nonetheless, theoretical calculations showed that the calculated energy of the second 6^+ level, 6_2^+, at 1785 keV was very close to the experimental energy of 1761.5 keV, whereas the calculated energy of the second 7^+ level, 7_2^+, at 2231 keV is ≈ 500 keV higher than the experimental energy. Based on these results, the spin of the 1761.5 keV level was considered to be $J = 6$, and a tentative $J^\pi = (6)^+$ was assigned to it.

The spin and parity of the 3747.2 keV level were not confirmed/assigned in the present work due to weak statistics of the feeding or decay out transitions. Its spin and parity were assigned $J^\pi = (9^+)$ tentatively based on the results of shell model calculations.

Five other transitions, viz., 1526, 2095, 2139, 2206, and 2286 keV, were seen in the 910.4 keV gated spectrum. These are marked with blue diamonds in the spectrum of Fig. 3(b). The 1526 and 2095 keV transitions were also seen in the 754 and 814.7 keV gated spectra. However, their coincidence relationships with other transitions in ^{50}V could not be established due to their weak statistics. These transitions were, therefore, not placed in the present level scheme of ^{50}V (Fig. 5).

In the present work, the mixing ratios of the dipole transitions were not extracted due to the large uncertainties in the reported δ's of 754 and 910.4 keV transitions. The 1725.1 keV ($8_1^+ \rightarrow 6_1^+$) gated spectrum was also not used for measuring mixing ratios due to low statistics.

Uncertainties quoted in the measured values of intensities and branching ratios include statistical errors, efficiency correction, and angular distribution correction for the intensities measured with the 90° detectors. In R_{DCO} measurements, uncertainties due to statistical errors and efficiency correction were considered. Uncertainties quoted in the Δ_{IPDCO} values are statistical only. Errors due to energy calibration and fitting errors were considered to estimate the uncertainty in the transition energy.

B. Lifetime measurements

The lifetimes of eight levels in ^{50}V were measured in the present work using line-shape analysis. Doppler-shifted line-shape spectra obtained from the 125° and 90° clovers were used in the present analysis. Although a clover was present at 40° during the experiment, its spectra were not considered in the analysis due to low statistics of the transitions of interest. Since, the line-shape spectra are generated by putting gates on a transition below the transitions of interest (discussed below), the effect of side feeding was properly considered and it was modeled with a cascade of five transitions or with a single-step feeding, depending on the type of transition of interest. The dynamic moment of inertia of the side-feeding band was considered accordingly. The side-feeding intensities were estimated from the relative intensities of the feeding and decay-out transitions. During each line-shape simulation, the transition quadrupole moments (Q_t), the side-feeding quadrupole moments (Q_{ts}) or the side-feeding times (τ_{ts}), and the background parameters for each level were kept as free parameters.

Of the eight levels, lifetime measurements of the 2313.2, 2841.2, 4088.3, and 5768.3 keV levels were carried out for the first time. Energy spectra of γ-ray transitions decaying from these four levels had large Doppler shifts (Fig. 6). The line-shape spectra of the decay-out 588.1 and 1930.8 keV transitions were generated by gating the 910.4 keV transition. As no transition could be found feeding the 2313.2 keV level, only an upper limit of its lifetime could be estimated. 754 keV gated spectra were used for the line-shape analysis of the decay-out 1609.2 and 1680 keV transitions (Fig. 6). The results of these four first-time measurements are summarized in Table II.

The lifetimes of four other levels, viz., 1725.1, 2479.1, 3730.5, and 4293.4 keV, were also remeasured in the present work. 910.4 keV gated spectra were used to generate the line-shape spectra of the 814.7, 754, 1251.4, and 562.9 keV transitions. Starting with the 562.9 keV transition, the 1251.4, 754, and 814.7 keV transitions were fitted sequentially, following which a global least-squares minimization was carried out for all four transitions simultaneously (Fig. 7). As no transition was found feeding the 4293.4 keV level, only an upper limit of its lifetime was estimated. These results are presented in Table II. In the same table, the previously measured lifetimes [15] of the four levels are also tabulated for comparison. Our results agree with these previous measurements (within the uncertainty limits). Another result for the lifetime of the 1725.1 keV was also reported by Kennedy *et al.* [16]. This reported lifetime does not agree with the result of our measurement or with that of Giorni *et al.* [15] (Table II). It may be noted here that the results of Ref. [15] contain significant uncertainties, more than 100% in most cases. The present work reports the four previously measured lifetimes with increased precision.

The quoted errors in the measured lifetimes were estimated from the behavior of the χ^2 fit in the vicinity of the minimum, stopping power uncertainties, and the continuous production and stopping of the recoils in the thick target and vacuum.
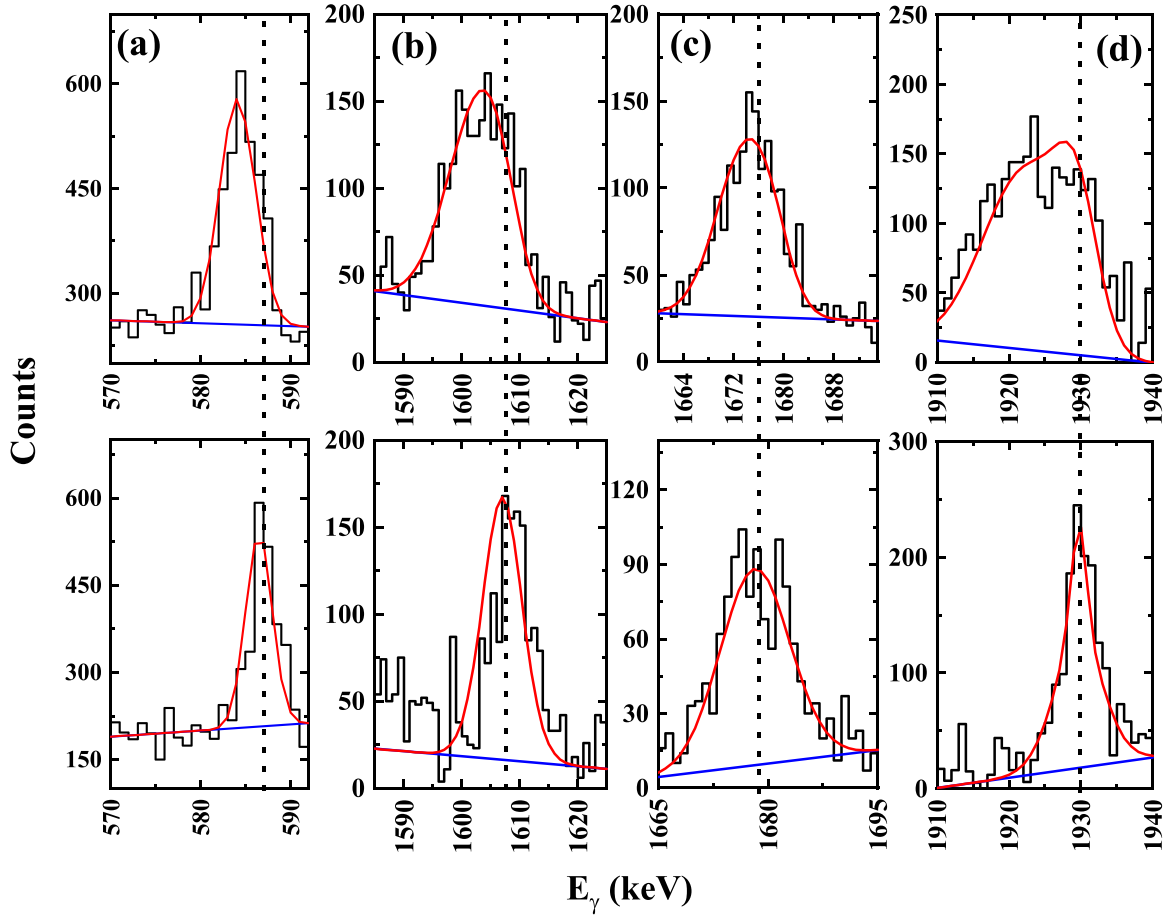
FIG. 6. Experimental (black) and simulated (red) line-shape spectra for (a) 588.1, (b) 1609.2, (c) 1680, and (d) 1930.8 keV transitions for two different angles, 125° (top) and 90° (bottom).

Experimental $B(M1)$ and $B(E2)$ values were then determined from these measured lifetimes. The branching ratios were taken from the present measurement. For the ground state positive parity band, the mixing ratios of the 910.4, 814.7, 754, 1251.4, and 562.9 keV transitions were taken from an earlier measurement [15]. For the other three magnetic dipole transitions (viz., 588.1, 1930.8, and 1609.2 keV), mixing ratios were taken from shell model calculations. The results are tabulated in Table II.

IV. THEORETICAL CALCULATION

LBSM calculations were performed using the code NUSHELLX [35] to understand the microscopic origin of the levels of interest in ^{50}V. The KB3G [36] effective interaction, developed for the fp major shell above ^{40}Ca core, was used for present calculations. The valence space consisted of the full fp major shell with $1f_{7/2}$, $1f_{5/2}$, $2p_{3/2}$, and $2p_{1/2}$ orbitals for both protons and neutrons above the ^{40}Ca inert core. The calculations were performed without any particle restrictions in the fp valence space. In the following subsections, theoretical results obtained from shell model calculations are discussed alongside the experimental results.

A. Level scheme

To begin with, the energies of the excited levels were obtained from LBSM calculations. A comparison with the experimental energies is shown in Fig. 8. The calculated energies of the levels of interest are in agreement with the experimental energies. During the calculation, special care was taken to compare the experimental and theoretical 7^+ levels as discussed below. In the discussions that follow, the nth occurrence of an energy level (arranged in order of increasing excitation energies) having a particular spin-parity J^π is denoted by a subscript n, viz., J_n^π.

The calculated energies of the 7_1^+ and 7_2^+ levels were in agreement with their corresponding experimental energies at 910.4 and 2313.2 keV, respectively. However, the calculated energy of the 7_3^+ level was found to be 2505 keV, ≈ 1 MeV less than the energy of the next experimental 7^+ level at 3475.4 keV. On the other hand, the calculated energies of the 7_4^+ and 7_5^+ levels were 3381 and 3542 keV, respectively, relatively closer to the energy of the next experimental 7^+ level. The experimental 7^+ level at 3475.4 keV decays to the ground state 6_1^+ and first excited state 7_1^+ via 3475 and 2565 keV transitions, with measured branching ratios 65(6) and 35(6), respectively. In order to find the correct positions of
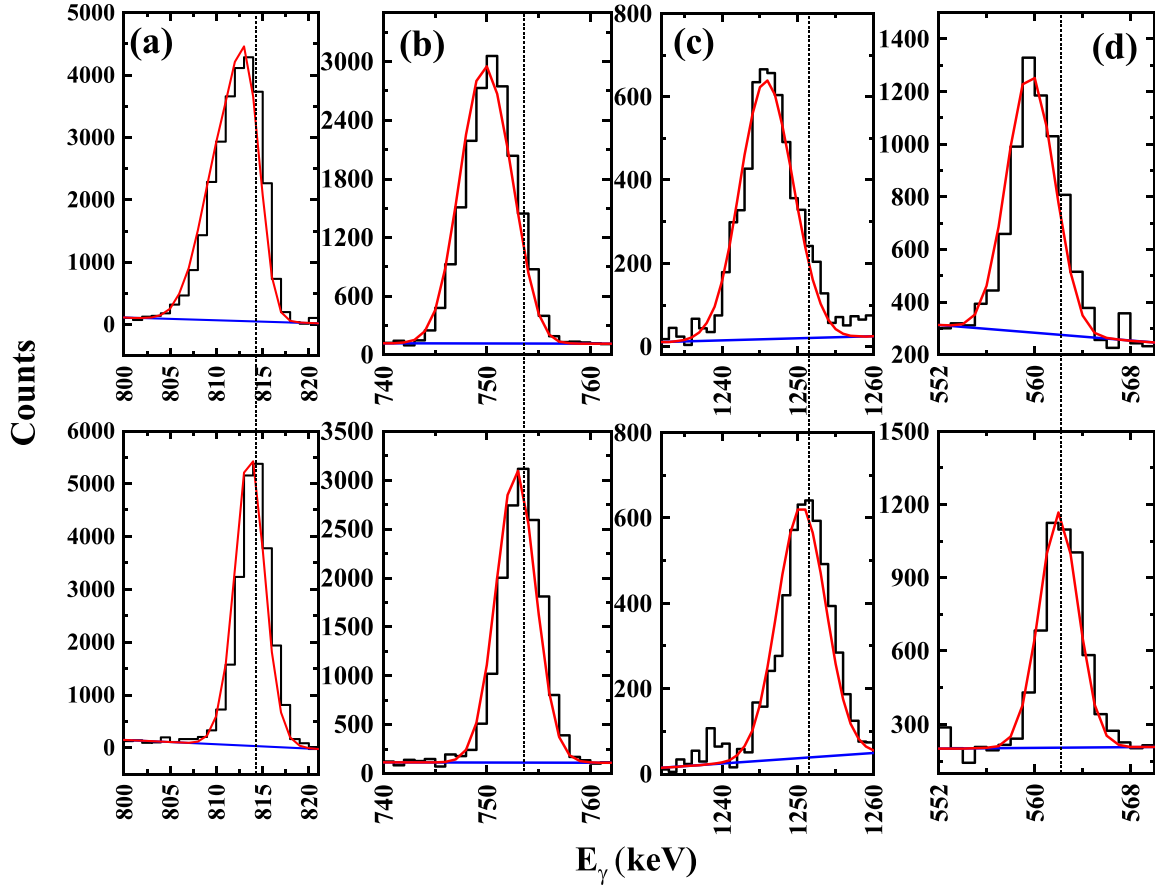
FIG. 7. Experimental (black) and simulated (red) line-shape spectra for (a) 814.7, (b) 754, (c) 1251.4, and (d) 562.9 keV transitions for two different angles, 125° (top) and 90° (bottom).

the theoretical levels, the branching ratios of $7^+ \rightarrow 6_1^+$ and $7^+ \rightarrow 7_1^+$ transitions were calculated considering both 7_4^+ and 7_5^+ levels. The calculated branching ratios for the $7_4^+ \rightarrow 6_1^+$ and $7_4^+ \rightarrow 7_1^+$ transitions were 4% and 96%, respectively, significant deviations from the experimental values. On the other hand, branching ratios of $7_5^+ \rightarrow 6_1^+$ and $7_5^+ \rightarrow 7_1^+$ transitions were calculated to be 81% and 19%, respectively, close to the experimental branching ratios. These findings led to the comparison of the experimental 3475.4 keV level with the theoretical 7_5^+ level at 3542 keV.

Additionally, the calculated transition energies of the $7_4^+ \rightarrow 7_1^+$ and $7_3^+ \rightarrow 8_1^+$ decays were 2446 and 635 keV with branching ratios 96% and 65%, respectively. Although a few transitions in these energy domains were seen in the 910.4 keV gated spectrum [marked by blue diamonds in Fig. 3(b)], they could not be identified due to low population yield of ^{50}V as well as due to weak intensities of the decay out transitions. Thus, it may be inferred that the 7_3^+ and 7_4^+ levels may be present in the level scheme of ^{50}V.

We have also extended our theoretical investigations for other J_n^{π}, viz., 5_3^+ or 9_2^+ of 3475.4 keV level. The result shows that both the cases, the level energies are largely deviated from their calculated energies obtained from shell model calculations (Fig. 9). The measured branchings of 2565 and 3475 keV transitions for $J^{\pi} = 5_3^+$ are also not reproduced. Since,

we could not calculate $M3$ transition strengths theoretically, a comparison between experimental and theoretical branchings of 2565 and 3475 keV transitions was not done for $J^{\pi} = 9_2^+$.

The $B(M1)$ and $B(E2)$ strengths of the decay out transitions in ^{50}V were also calculated from the wave functions of the levels of interest. Effective charges $e_p = 1.5e$ and $e_n = 0.5e$ [37], and the free values of g-factors were used in the calculation. The calculated $B(M1)$ and $B(E2)$ strengths are compared with their present experimental values in Table II. The transition strengths of the transitions decaying through the newly identified non-yrast band were also calculated. These calculated transition strengths were then used to estimate the level lifetimes of the non-yrast band in ^{50}V (Table II). As the multipole mixing ratios of the transitions in the non-yrast band were not known, the calculated multipole mixing ratios of Table II were used to estimate the lifetimes of the levels.

B. Particle partitions and configuration mixing

The decomposition of wave functions of the positive-parity levels in ^{50}V are shown in Table III. The partitions are written in terms of occupation numbers of the valence single-particle orbits, and N is the total number of particle partitions involved in a particular level. The average occupancies of protons and
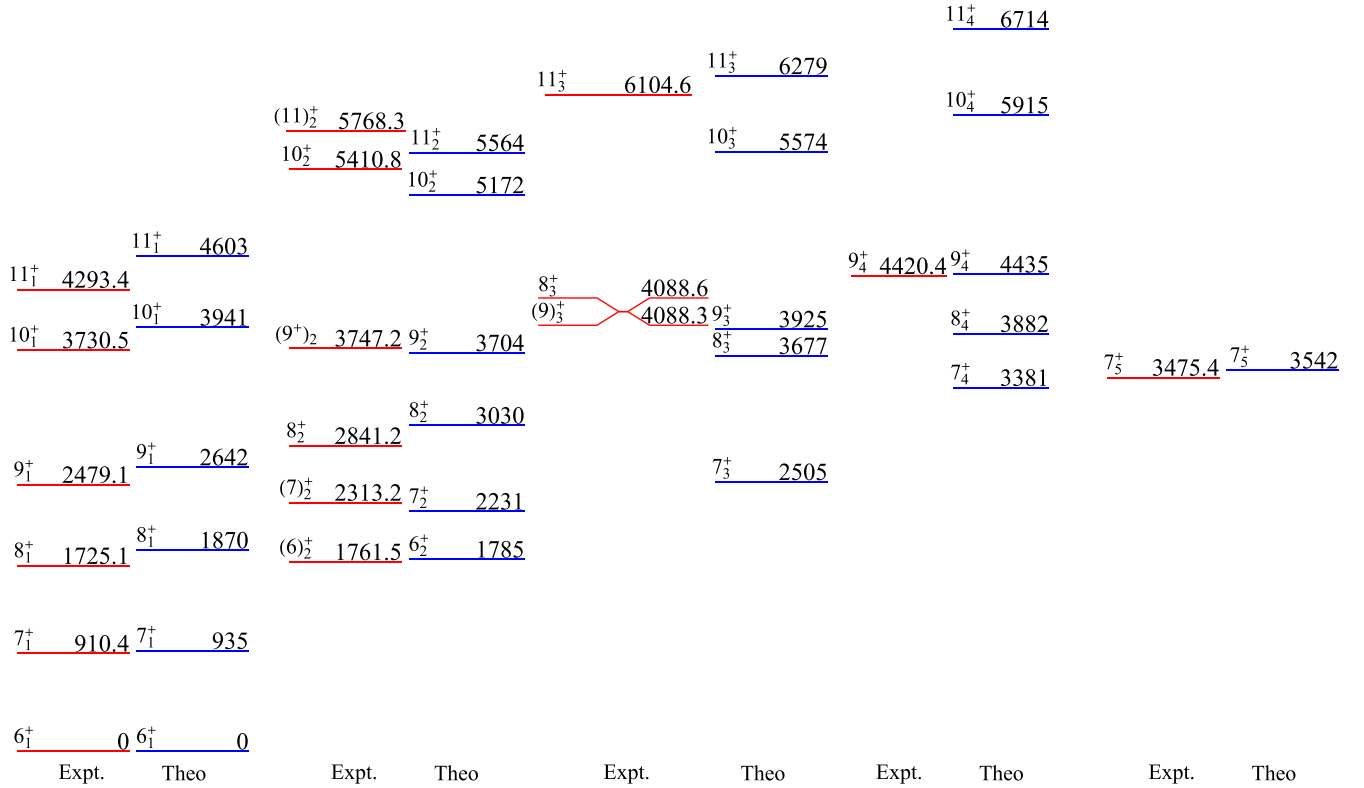
FIG. 8. Comparison of theoretical and experimental level schemes for the positive parity states of interest in ^{50}V. All these energies are plotted considering the ground state energy (-116.582 MeV) as 0.

neutrons in the fp orbitals for the ground state yrast band and the non-yrast band of ^{50}V are plotted in Fig. 10.

Table III and Fig. 10 show that the ground state band was primarily generated from a $\pi(1f_{7/2}^3) \otimes \nu(1f_{7/2}^7)$ particle configuration and had a much smaller extent of configuration mixing. It was found that the low-lying levels of this band had comparatively larger configuration mixing in terms of
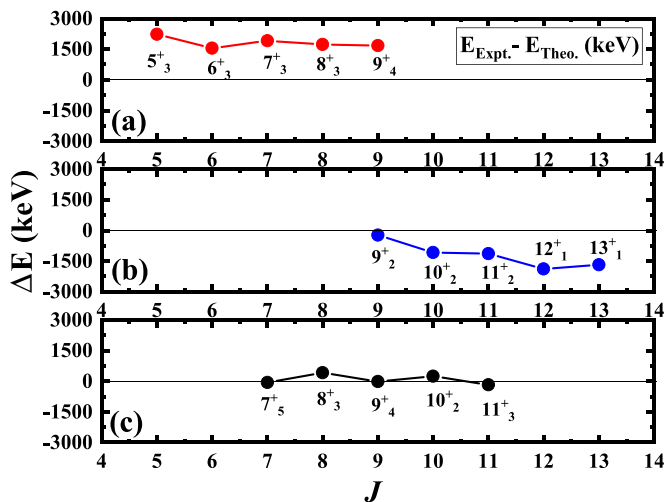

FIG. 9. Deviation between the experimental and theoretical level energies for $J^{\pi} =$ (a) 5_3^+, (b) 9_2^+, and (c) 7_5^+ of the 3475.4 keV level. Data points are connected by lines to aid the eye.

single-particle partitions, which showed a decreasing trend with increasing angular momenta. The minimum configuration mixing with the largest contribution from a single partition ($\approx 71\%$) was obtained for the 11_1^+ level, the band-terminating state of the observed positive parity yrast band.

The observed non-yrast band with a 7_5^+ bandhead spin was primarily generated with a $\pi(1f_{7/2}^3) \otimes \nu(1f_{7/2}^6, 2p_{3/2}^1)$ particle configuration (Table III and Fig. 10), and had a much larger extent of configuration mixing. The low lying levels in this band had comparatively larger configuration mixing in terms of single-particle partitions ($N_{\max} = 126$), which also showed a decreasing trend with increasing angular momenta. The 11_3^+ level showed the minimum configuration mixing with the largest contribution from a single partition ($\approx 48\%$).

Large configuration mixings (≈ 36–58%) were also found for the other observed non-yrast levels in ^{50}V (Table III).

C. Spectroscopic quadrupole moments (Q_s) and g factors

In the present study, the spectroscopic quadrupole moments (Q_s) and g factors of the levels of ^{50}V were calculated from their wave functions obtained from shell model calculations. These are tabulated in Table IV. For the non-yrast band, Q_s's were positive, with the maximum value for the bandhead. Q_s's then decreased to 14–15 e fm^2 at higher angular momenta. For the ground state yrast band, the Q_s of the ground state was $+20.8$ e fm^2, which then decreased to -10.7 e fm^2 at the band-terminating state, 11^+. A sudden change in Q_s

TABLE III. Structure of wave functions of the levels of interest in ^{50}V. The partitions are given in terms of occupation numbers of the valence single-particle states in the following order: $\pi\, 1f_{7/2}$, $\pi\, 2p_{3/2}$, $\pi\, 1f_{5/2}$, $\pi\, 2p_{1/2}$, $\nu\, 1f_{7/2}$, $\nu\, 2p_{3/2}$, $\nu\, 1f_{5/2}$, and $\nu\, 2p_{1/2}$. T is the isospin label of the levels and N is the total number of particle partitions contributing to the corresponding level.

J_i^π	T	Energy (MeV)		Wave function		N
		Expt.	Theor.	%	Partition	
For ground state yrast band						
6_1^+	2	0	0	58	[3,0,0,0,7,0,0,0]	68
7_1^+	2	910.4	935	61	[3,0,0,0,7,0,0,0]	62
8_1^+	2	1725.1	1870	61	[3,0,0,0,7,0,0,0]	66
9_1^+	2	2479.1	2642	60	[3,0,0,0,7,0,0,0]	61
10_1^+	2	3730.5	3941	64	[3,0,0,0,7,0,0,0]	47
11_1^+	2	4293.4	4603	71	[3,0,0,0,7,0,0,0]	42
For non-yrast band						
7_5^+	2	3475.4	3542	39	[3,0,0,0,6,1,0,0]	117
8_3^+	2	4088.6	3677	38	[3,0,0,0,6,1,0,0]	126
9_4^+	2	4420.4	4435	47	[3,0,0,0,6,1,0,0]	113
10_2^+	2	5410.8	5172	52	[3,0,0,0,6,1,0,0]	97
11_3^+	2	6104.6	6279	48	[3,0,0,0,6,1,0,0]	97
For other non-yrast levels						
$(6)_2^+$	2	1761.5	1785	49	[3,0,0,0,7,0,0,0]	81
$(7)_2^+$	2	2313.2	2231	36	[3,0,0,0,6,1,0,0]	94
8_2^+	2	2841.2	3030	58	[3,0,0,0,7,0,0,0]	75
$(9^+)_2$	2	3747.2	3704	40	[3,0,0,0,6,1,0,0]	83
$(9)_3^+$	2	4088.3	3925	46	[3,0,0,0,7,0,0,0]	80
$(11)_2^+$	2	5768.3	5564	56	[3,0,0,0,6,1,0,0]	74

was also observed at $J^\pi = 9_1^+$. The $(9^+)_2$ and $(9)_3^+$ levels decay to the 9_1^+ level through 1268.1 and 1609.2 keV transitions, respectively, with negative Q_s values (Table IV). The

TABLE IV. Spectroscopic quadrupole moments (Q_s), and g factors of ^{50}V calculated from LBSM calculations. The unit of Q_s is $e\,\mathrm{fm}^2$.

J^π	Q_s	g factor
For ground state yrast band		
6_1^+	20.8	0.53
7_1^+	7.0	0.59
8_1^+	10.3	0.76
9_1^+	−28.3	0.76
10_1^+	−13.3	0.86
11_1^+	10.7	0.85
For non-yrast band		
7_5^+	45.9	0.30
8_3^+	45.3	0.18
9_4^+	28.3	0.22
10_2^+	14.4	0.27
11_3^+	15.2	0.37
For other non-yrast levels		
$(6)_2^+$	−12.3	0.58
$(7)_2^+$	−16.1	0.66
8_2^+	10.3	0.69
$(9^+)_2$	−19.7	0.66
$(9)_3^+$	−13.8	0.77
$(11)_2^+$	−21.1	0.49

change in Q_s at 9_1^+ could be due to a mixing between these levels.

The calculated spectroscopic quadrupole moments were compared with the values obtained for a rigid rotor using the relations mentioned in Ref. [38] for both bands (Fig. 11). The parameter $\beta^\star$ [$\beta^\star = \beta(1 + 0.36\beta)$, with β as the deformation parameter] was taken as 0.10 and 0.25 for the ground state yrast band and the non-yrast band, respectively. These results show that the non-yrast band has a larger deformation com-

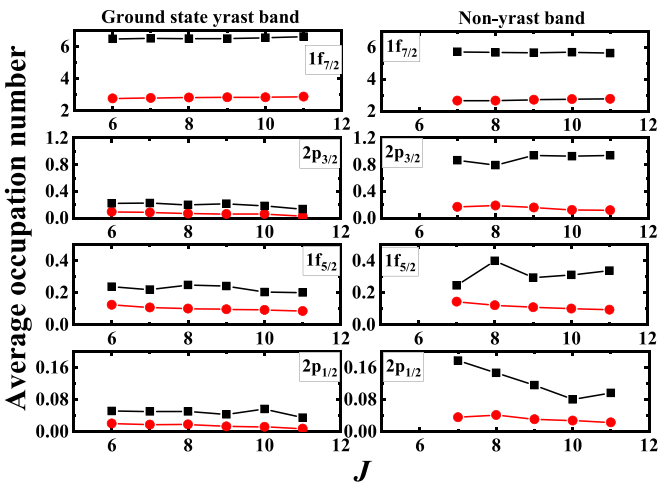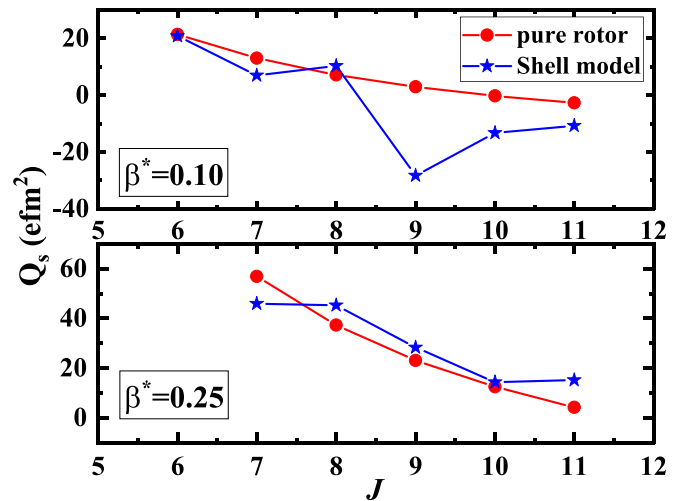
FIG. 10. The average calculated occupation numbers of $1f_{7/2}$, $2p_{3/2}$, $1f_{5/2}$, and $2p_{1/2}$ orbitals (top to bottom panels) for the positive parity levels of the ground state yrast band and the non-yrast band (left to right panels) of ^{50}V. The calculated proton and neutron occupation numbers are represented as red circles and black squares, respectively. Data points are connected by lines to aid the eye.

FIG. 11. Comparison of spectroscopic quadrupole moment (Q_s) of the levels obtained from shell model calculations and from pure rotor model for the ground state yrast band (top) and the non-yrast band (bottom). Data points are connected by lines to aid the eye.

pared to the ground state yrast band, as also suggested by the particle partitions obtained from shell model calculations (Table III).

V. CONCLUSION

High-spin states of ^{50}V, populated through a ^{48}Ti(^{4}He, np) ^{50}V reaction at $E_{\text{lab}} = 48$ MeV, were studied using the INGA facility. The level scheme was modified by adding eight new levels and thirteen new γ-ray transitions to the existing level scheme. Relative intensity, directional correlation, and polarization measurements were carried out for the decay out transitions to assign/confirm the spins and parities of the levels. The lifetimes of four levels were measured for the first time using the Doppler shift attenuation method. In addition, lifetimes of four other levels were remeasured with increased accuracies compared to earlier measurements. Reduced transition probabilities were extracted from the measured branching ratios and lifetimes. Large basis shell model calculations were performed to

understand the microscopic origin of the levels. The interplay between single-particle and collective modes of excitation were studied based on the results of shell model calculations.

[1] S. M. Lenzi, in *Nuclear Physics with Stable and Radioactive Ion Beams, Proceedings of the International School of Physics "Enrico Fermi"*, edited by F. Gramegna, P. Van Duppen, A. Vitturi, and S. Pirrone (IOS, Amsterdam, 2019).

[2] S. M. Lenzi *et al.*, Z. Phys. A-Hadrons and Nuclei **354**, 117 (1996).

[3] J. A. Cameron *et al.*, Phys. Lett. B **387**, 266 (1996).

[4] S. M. Lenzi *et al.*, Phys. Rev. C **56**, 1313 (1997).

[5] J. A. Cameron, M. A. Bentley, A. M. Bruce, R. A. Cunningham, W. Gelletly, H. G. Price, J. Simpson, D. D. Warner, and A. N. James, Phys. Rev. C **49**, 1347 (1994).

[6] C. E. Svensson *et al.*, Phys. Rev. C **58**, R2621(R) (1998).

[7] F. Brandolini *et al.*, Nucl. Phys. A **642**, 387 (1998).

[8] E. Caurier, G. Martinez-Pinedo, F. Nowacki, A. Poves, and A. P. Zuker, Rev. Mod. Phys. **77**, 427 (2005).

[9] A. P. Zuker, Phys. Rev. Lett. **90**, 042502 (2003).

[10] G. Martínez-Pinedo, A. Poves, L. M. Robledo, E. Caurier, F. Nowacki, J. Retamosa, and A. Zuker, Phys. Rev. C **54**, R2150(R) (1996).

[11] Y. Sapkota *et al.*, Phys. Rev. C **105**, 044304 (2022).

[12] H. Ohmura *et al.*, Phys. Lett. B **73**, 145 (1978).

[13] R. DelVecchio *et al.*, Phys. Rev. C **3**, 1989 (1971).

[14] H. Sekiguchi, J. Phys. Soc. Jpn. **26**, 589 (1969).

[15] A. Giorni *et al.*, Nucl. Phys. A **292**, 213 (1977).

[16] D. L. Kennedy *et al.*, Nucl. Phys. A **293**, 150 (1977).

[17] T. Caldwell, O. Hansen, and D. J. Pullen, Nucl. Phys. A **198**, 529 (1972).

[18] J. W. Smith *et al.*, Phys. Rev. C **7**, 1099 (1973).

[19] https://www.nndc.bnl.gov

[20] S. Das *et al.*, Nucl. Instrum. Methods Phys. Res., Sect. A **893**, 138 (2018).

[21] R. Bhowmick *et al.*, Proc. DAE-BRNS Symp. Nucl. Phys. B **44**, 422 (2001).

[22] A. Bisoi *et al.*, Phys. Rev. C **89**, 024303 (2014).

[23] E. S. Macias, W. D. Ruhter, D. C. Camp, and R. G. Lanier, Comput. Phys. Commun. **11**, 75 (1976).

[24] K. Starosta *et al.*, Nucl. Instrum. Methods A **423**, 16 (1999).

[25] R. Palit *et al.*, Pramana **54**, 347 (2000).

[26] R. Raut *et al.*, Proc. DAE-BRNS Symp. Nucl. Phys. B **47**, 578 (2004).

[27] S. Muralithar *et al.*, Nucl. Instrum. Methods Phys. Res., Sect. A **622**, 281 (2010).

[28] E. Der Mateosian *et al.*, At. Data Nucl. Data Tables **13**, 391 (1974).

[29] C. Wells and N. R. Johnson, ORNL Report No. 6689, 1991, p. 44; R. K. Bhowmik (private communication).

[30] A. Gavron, Phys. Rev. C **21**, 230 (1980).

[31] L. C. Northcliffe and R. F. Schilling, At. Data Nucl. Data Tables **7**, 233 (1970).

[32] F. Brandolini *et al.*, Phys. Rev. C **73**, 024313 (2006).

[33] A. Das *et al.*, Phys. Rev. C **101**, 044310 (2020).

[34] J. D. McCullen, B. F. Bayman, and L. Zamick, Phys. Rev. **134**, B515 (1964).

[35] W. D. M. Rae, NUSHELLX, http://www.garsington.eclipse.co.uk.

[36] A. Poves, J. Sánchez-Solano, E. Caurier, and F. Nowacki, Nucl. Phys. A **694**, 157 (2001).

[37] F. Brandolini *et al.*, Phys. Rev. C **66**, 024304 (2002).

[38] F. Brandolini and C. A. Ur, Phys. Rev. C **71**, 054316 (2005).